Design and Analysis of a Low-Speed and High-Torque Dual-Stator Permanent Magnet Motor With Inner Enhanced Torque

JIAXU ZHANG, BINGYI ZHANG, GUIHONG FENG, AND BAOPING GAN

School of Electrical Engineering, Shenyang University of Technology, Shenyang 110870, China

Corresponding author: Guihong Feng (78908410@qq.com)

ABSTRACT Given the problem that the drive system of the traditional mine transportation winch outputs a large traction force through the cooperation of an induction motor and reducer to meet the needs of a large traffic volume and heavy-load starting, this paper studies a low-speed and high-torque dual-stator permanent magnet direct drive motor with a separated magnetic circuit. The inner motor is a torque motor, and the outer motor is a direct drive motor, which is characterized by no magnetic circuit coupling and independent control. The proposed motor has an excellent heavy load starting ability and operation efficiency, and it improves the output torque without increasing the motor volume, which belongs to a special application. According to the working characteristics of the inner and outer motors and the constraints between the overall dimensions, the size equation is derived, and the design principles of the electromagnetic parameters, pole-slot combination and winding structure are described. The torque characteristics and temperature rise characteristics of the motor are simulated using the finite element method and compared with the torque performance and electromagnetic materials cost of the single stator low-speed and high-torque permanent magnet motor with different rotor structures. The results show that the proposed motor has a high torque density and starting torque, and it greatly reduces the motor volume on the basis of a small cost difference.

INDEX TERMS Enhance torque, dual-stator, motor design, finite element analysis, torque characteristics.

I. INTRODUCTION

The winch is essentially mechanical and electrical equipment in the mine track transportation. Its performance is directly related to the production efficiency. At present, the drive system of the mine winch generally adopts the method of a matching induction motor and reducer to achieve a larger torque output, which exposes the shortcomings of the existing winch in the running state. First, the presence of the reducer brings many disadvantages to the transmission system, such as a reduction of efficiency, increase in equipment volume and a daily maintenance workload, etc., and the mechanical differential mode has a poor speed regulation performance and cumbersome operation; second, the heavy-load starting of a winch often occurs. The moving process from static to motion requires that the drive motor has a large starting torque capacity, but after the winch is running, it does not need a high rated torque under the rated working condition.

The associate editor coordinating the review of this manuscript and approving it for publication was Shuaihu Li.

Therefore, a large power redundancy occurs in the selection of the motor and its controller, which is equivalent to a portion of motor power only used in the starting process, resulting in unnecessary waste of resources and an increase in cost. In addition, the efficiency of the motor decreases with the decrease in load.

Based on the above problems, this paper proposes a low-speed and high-torque dual-stator permanent magnet motor with inner enhanced torque. Many scholars have performed research on the dual-stator permanent magnet synchronous motor (DS-PMSM). In Ref. [1], a complete performance analysis of a double-stator starter generator for hybrid electric vehicles has been provided. Various types of DS-PMSM have been compared with each other, and the effects of the structural parameters on the ripple and average value of the torque have been investigated. In Ref. [2], the author presents a DS-PMSM with diametrically magnetized cylindrical PMs, and the rotor structure reduced the cogging torque and torque ripple without increasing the cost of construction. To improve the overload capacity of the wheel

motor, a dual-stator permanent magnet synchronous motor is introduced in Ref. [3], and from the power load, the torque characteristics of the motor are theoretically derived and simulated. A high-torque-density dual-stator permanent magnet machine with a biased permanent magnet (PM) excitation in the inner stator was proposed in Ref. [4]. In Ref. [5], a 600 kW, 60 r/min double-stator PMSM with a low- speed and high-torque is designed, including the choice of the topology of the motor and the electromagnetic and structural parameters. In Ref. [6], a high torque density, high power factor, low speed direct drive double-stator axial-flow permanent magnet motor is proposed, and its working principle and design method are introduced. The DS-FSPM is studied in Refs. [7] and [8] and compared with the conventional FPSM; the higher torque density of the proposed motor is proved. In Ref. [9], the authors improved the torque characteristics (regarding the value and cogging) of the two dual-stator, two-phase PMSMs using a phase-group concentrated-coil winding. In Ref. [10], a novel double-stator axial-flux spoke-type permanent magnet Vernier machine is proposed; it has a high torque density feature as well as a high-power factor at low speed for direct-drive systems. In Ref. [11], several factors that affect the torque of a double-stator motor are studied: the pole-arc width, pole number, length of the outer and inner air gap, tooth slot matching of the outer and inner stator and stator fission ratio. In Ref. [12], [13], the double-stator permanent magnet brushless motor used in the power distribution device of hybrid electric vehicles is studied, and the dimensional equation of the motor and the determination method of its main dimensions are analyzed.

The cogging torque, which results in shaft vibration and acoustic noise, especially at low speeds and direct-drive applications, is one of the primary drawbacks of these motors [14]. Analytical methods for minimizing the cogging torque in PM machines have been investigated in [14]–[16]. In Ref. [17], the phase of the cogging torque under different combinations of slot opening ratios and pole-arc ratios is analyzed. Based on this analysis, two techniques for minimizing the cogging torque of the axial-flux permanent-magnet machines are proposed and discussed. Ref. [18] proposes more methods for reducing the cogging torque, such as a relative position shift between the inner/outer magnet poles, inner/outer slot number pairing, size pairing of the inner/outer slot openings, and size pairing of the inner/outer pole-arc to pole-pitch ratios.

Most of the above papers are about the research and design of a dual-stator permanent magnet motor with a small rated torque, whereas research on a large-scale low-speed and high-torque permanent magnet direct drive motor is rarely considered. Therefore, this paper presents a dual-stator permanent magnet direct drive motor (DS-PMDDM) for use in a mine winch. Its characteristic is that the inner motor is a torque motor running briefly when the winch is started or overloaded, and the outer motor is a rated load driven by the direct drive motor. This operation mode not only solves

the problems of heavy load starting and overload operation of the winch but also makes DS-PMDDM work in a higher efficiency range when it drives a normal load for a long time. The inner and outer motors can be designed separately according to their working characteristics, which improves the utilization rate and design flexibility of the motor. The proposed motor not only changes the complex driving structure of the traditional winch and saves space but also has a good heavy load starting ability and operation efficiency, which solves the problems of the power redundancy and heavy load starting difficulty of the original motor, which has great significance for the mine winch drive system.
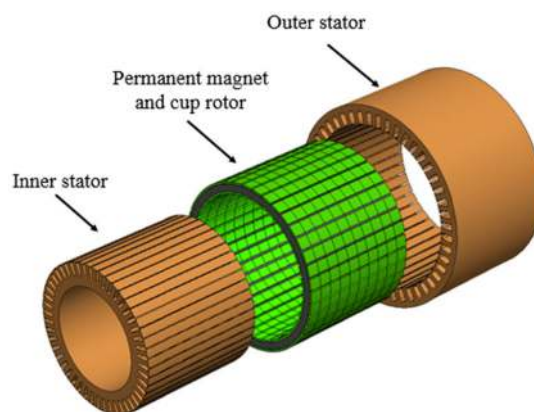

FIGURE 1. Structure diagram of DS-PMDDM.

II. STRUCTURE AND CHARACTERISTICS OF DS-PMDDM

Fig. 1 shows the structure diagram of DS-PMDDM, which is characterized by the full use of the inner space of the motor and can be considered the superposition of two permanent magnet motors. The magnetic pole adopts the surface stick separated magnetic circuit structure, the inner and outer stators and adjacent permanent magnet layers form a separate closed magnetic circuit, and there is no magnetic circuit coupling between the inner and outer machines, which can be independently controlled.

The air gap diameter of the outer motor is large and the water cooling of the outer casing is convenient, so the higher electric and magnetic loads can be selected. Therefore, the outer motor is used as the permanent magnet direct drive motor, which directly drives the rated load of the winch; the inner motor is used as the torque motor for short-time operation, which is used as the auxiliary motor when the winch is started, braked or overloaded. Because the inner motor is only used as an auxiliary motor for short-time operation, the selection of its thermal load is higher than that of the conventional motor in design, so its torque density is also improved.

III. STUDY AND DESIGN OF DS-PMDDM

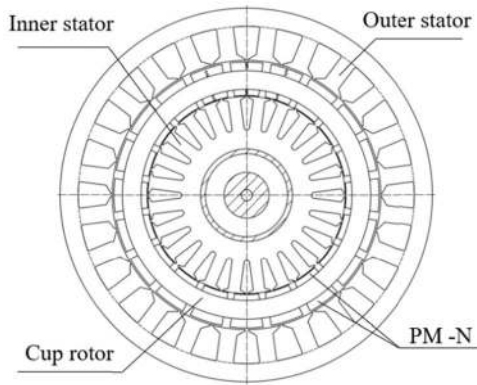The radial section of the DS-PMDDM is shown in Fig. 2. As analyzed above, the magnetic circuit structure adopted

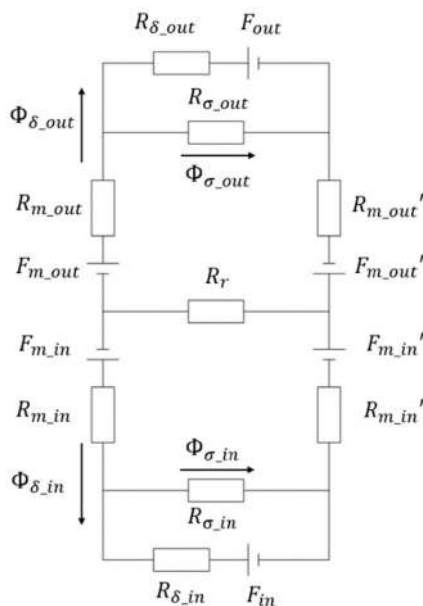**FIGURE 2.** Radial section of the DS-PMDDM.

FIGURE 3. Load equivalent circuit diagram of the DS-PMDDM.

in this paper is a separate parallel magnetic circuit. The inner and outer permanent magnets are on the same axis with opposite magnetization directions, the pole and slot number matchings of the inner and outer motors are identical, the teeth are aligned and the poles are identical. The load equivalent circuit diagram of the DS-PMDDM is shown in Fig. 3. It is apparent that, unlike the traditional PMSM with a single stator structure, the DS-PMDDM has independent windings on the inner and outer stators. When the inner and outer stator windings are energized, they generate the rotating magnetomotive forces F_{in} and F_{out} and establish an armature magnetic field, ignoring the effect of armature reaction; the inner and outer magnetic steels of the rotor generate the magnetomotive forces F_{m_in} and F_{m_out} and establish an excitation magnetic field. The resultant inner and outer air gap magnetic fields generate back EMF in the inner and outer stator windings, respectively. Therefore, the inner and outer stator windings of the DS-PMDDM work together to produce a superposition performance.

In Fig. 3, ϕ_{δ_out} and ϕ_{σ_out} are the main flux and leakage flux of the outer motor respectively, R_{m_out} is the internal reluctance of the PM, R_{δ_out} is the main reluctance including the air gap and stator teeth and yoke, R_r is the rotor reluctance, and R_{σ_out} is the leakage reluctance. When in the no-load condition, i.e., when F_{in} and F_{out} equal 0, the calculation formula of the main flux path of the outer motor is shown in Eq. (1). Because the inner and outer motors adopt a parallel magnetic circuit, and the magnetic circuit is symmetrical, the flux calculation expression of the inner motor is identical to that of the outer motor, except that the values of the permeance and magnetic potential parameters of each part are different.

$$(\phi_{\delta\_out} + \phi_{\sigma\_out})[2R_{m\_out} + R_r + (R_{\delta\_out}^{-1} + R_{\sigma\_out}^{-1})^{-1}]$$
$$= 2H_c h_{m-out} \quad (1)$$

where H_c is the coercivity of the permanent magnet, and h_{m_out} is the thickness of the outer motor permanent magnet.

In the permanent magnet motor, the leakage field distribution is very complex, so it is difficult to calculate the leakage permeance accurately. For a surface mounted permanent magnet motor, there is a small amount of flux leakage between each pair of PMs. The magnetic leakage resistance is far greater than that of the main flux path, and the permeability of the stator core and rotor core is far greater than that of the air permeability. To facilitate the calculation, a part of the magnetoresistance is ignored, and Eq. (1) can be further simplified because the air gap flux density of the motor can be obtained from the magnetic flux:

$$\phi_{\delta\_out} = \frac{2H_c h_{m-out}}{2R_{m\_out} + R_{\delta\_out}} \quad (2)$$

$$R_{m\_out} = \frac{h_m}{\mu_0 \mu_r A_m} \quad (3)$$

The air gap magnetoresistance expressed by air gap parameters and magnetic circuit saturation is as follows:

$$R_{\delta\_out} = \frac{2g_1 K_\delta K_s}{\mu_0 A_\delta} \quad (4)$$

where A_m is the upper cross-sectional area of the permanent magnet perpendicular to the magnetizing direction, μ_0 is the vacuum permeability, μ_r is the relative permeability of the permanent magnet, g_1 is the length of the outer air gap, K_δ is the air gap coefficient, K_s is the saturation coefficient, and A_δ is the effective area of each pole air gap.

A. DIMENSION EQUATION AND CONSTRAINT OF DS-PMDDM

Because the outer motor is used as a permanent magnet direct drive motor for normal operation, it must meet the given winch rated operation parameters and installation dimensions. As an auxiliary torque motor, the inner motor is designed and optimized on the basis of the main dimension parameters of the outer motor. Ignoring the influence of winding leakage inductance and armature reaction, the relationship between the PMSM electromagnetic torque and the

motor electromagnetic load and main dimensions is [19]:

$$T_{em} = \frac{\pi \sqrt{2}}{4} B_\delta L_{ef} D_{i1}^2 K_{dp1} A \qquad (5)$$

where B_δ is the air gap flux density, L_{ef} is the effective core length, D_{i1} is the armature diameter, K_{dp1} is the winding factor, and A is the specific electric loading of the motor.

$$A = \frac{2mNI}{\pi D_{i1}} \qquad (6)$$

where m is the number of phases, N is the number of series turns of each phase winding, and I is the effective value of the rated current.

For the convenience of analysis, when the inner and outer motors are designed with the same air gap flux density, the expression for the electromagnetic torque when the inner and outer motors of the DS-PMDDM are working at the same time is as follows:

$$T_{em} = \frac{\pi \sqrt{2}}{4} B_\delta L_{ef} K_{dp1}(A_1 D_{i1\_out}^2 \pm A_2 D_{i1\_in}^2) \qquad (7)$$

Eq. (7) shows that the total electromagnetic torque of the DS-PMDDM is provided by the inner and outer motors together, and the contribution of the inner and outer motor electromagnetic torque is determined by its specific electric loading and armature diameter, where the sign is determined by the electromagnetic torque property of the inner motor.

The output power P of the motor is expressed as follows:

$$P = T_{em} \, \Omega \qquad (8)$$

where Ω is the mechanical angular speed of the rotor.

The dimension equation of the DS-PMDDM outer motor can be obtained from Eq. (5) and Eq. (8):

$$D_{i1\_out}^2 L_{ef} = \frac{P_{o1}}{\frac{\pi \sqrt{2}}{4} \Omega B_{\delta 1} K_{dp1} A_1} \qquad (9)$$

where P_{o1} is the output power of the outer motor, D_{i1_out} is the inner diameter of the outer stator, A_1 is the specific electric loading of the outer motor, and $B_{\delta 1}$ is the flux density of the outer air gap.

Similarly, the size equation of the inner motor can be obtained:

$$D_{i1\_in}^2 L_{ef} = \frac{P_{o2}}{\frac{\pi \sqrt{2}}{4} \Omega B_{\delta 2} K_{dp1} A_2} \qquad (10)$$

where P_{o2} is the output power of the inner motor, D_{i1_in} is the outer diameter of the inner stator, and A_2 is the specific electric loading of the inner motor.

At the same time, the inner and outer motor armature diameters have the following dimensional constraints:

$$D_{i1\_in} = D_{i1\_out} - 2(h_{jr} + h_{m\_in} + h_{m\_out} + g_1 + g_2) \qquad (11)$$

where h_{jr} is the thickness of the rotor yoke, h_{m_in} and h_{m_out} are the thickness of the inner and outer motor permanent magnets, respectively, g_1 is the length of the outer air gap, and g_2 is the length of the inner air gap.

Eqs. (10) and (11) show that, when the diameter of the outer stator armature is determined, the rated power and output torque of the inner motor completely depend on the design of its magnetic circuit parameters and have greater flexibility.

Because of the different working characteristics of the inner and outer motors, the thermal load of the motor is taken according to its operating conditions and cooling mode. The thermal load Q of the motor is the product of the specific electric loading and electric density, which can be expressed as follows:

$$Q_1 = A_1 J_1 \qquad (12)$$
$$Q_2 = A_2 J_2 \qquad (13)$$

where J_1 and J_2 are current density of outer motor and inner motor respectively.
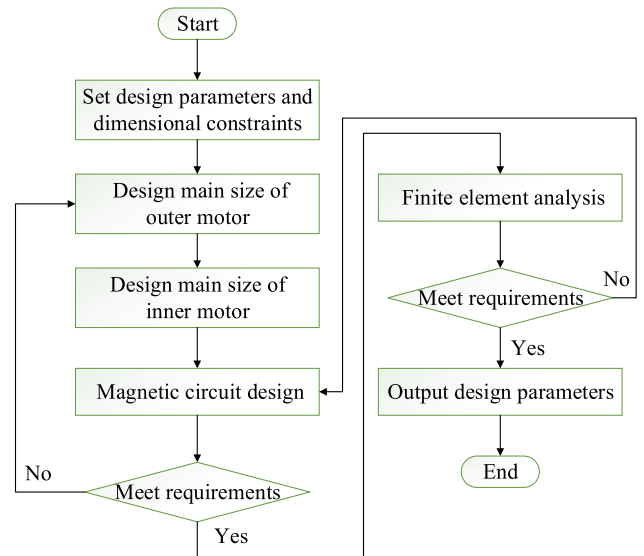

FIGURE 4. Design flow chart of the DS-PMDDM.

B. DESIGN PROCESS OF THE DS-PMDDM

The design flow chart of the DS-PMDDM is shown in Fig. 4. Based on the given winch installation dimension, namely, the outer motor stator outer diameter and the rated operation parameters, and based on the derived dimension equation, the key dimension parameters, such as the outer motor stator outer diameter, inner diameter and core length, are preliminarily determined. Then, according to the constraint equation of the armature diameter of the inner and outer motors, and the value range of the inner and outer motor thermal load determined according to the motor working characteristics, through a linear magnetic circuit calculation, magnetic circuit parameters, such as the air gap length, thickness of the permanent magnet, number of series turns of each phase winding and pole embrace of the permanent magnet, are designed and optimized.

C. POLE-SLOT COMBINATION AND WINDING STRUCTURE

Because of the low operating speed of the winch, the permanent magnet direct drive motor must be designed into

a multipoles structure to achieve a lower speed. Because of the numerous rotor poles, the magnetic density of the stator yoke is relatively low compared with that of the teeth, so the thickness of the stator yoke can be designed smaller, but the premise is to meet the requirements of mechanical strength to prevent the deformation of the motor stator in the process of press mounting.

The DS-PMDDM proposed in this paper adopts a fractional slot concentrated winding with near pole slot coordination. The coil pitch is 1, and the winding pitch coefficient is high [20], [21]. For a fractional slot concentrated winding, the number of slots per phase per pole q is expressed as follows:

$$q = \frac{Z}{2mp} = \frac{N}{d} \tag{14}$$

where N/d is the irreducible true fraction, m is the number of phases, Z is the number of stator slots, and p is the pole pairs.

In general, there is a greatest common divisor t between the slots Z and pole pairs p of the fractional slot concentrated winding motor, that is

$$t = \frac{Z}{p} = \gcd(Z, p) \tag{15}$$

If $Z_0 = Z/t$ and $p_0 = p/t$, then q can be rewritten as follows:

$$q = \frac{Z_0}{2mp_0} \tag{16}$$

Therefore, the motor with Z_0 slots and p_0 pole pairs is called a unit motor, and the original motor consists of t unit motors.

For the DS-PMDDM, the different pole-slot combinations can be selected for the inner and outer motors. As the parallel separated magnetic circuit structure is adopted in the motor proposed in this paper, the poles of the inner and outer motors are identical and coincident with the d-axis, so when the q of the inner and outer motors are different, the pole pairs of the DS-PMDDM is the lowest common multiple of the pole pairs of the inner and outer unit motors and its integer multiple.

$$p = k \cdot \text{lcm}(p_{01}, p_{02}) \tag{17}$$

where p is the pole pairs of the DS-PMDDM, p_{01} and p_{02} are the pole pairs of the inner and outer unit motors, respectively, and k is a positive integer.

For example, if the pole pairs of the outer unit motor $q_{01} = 2/5$ and the pole pairs of the inner unit motor $q_{02} = 3/8$, then the minimum pole pairs of the DS-PMDDM is 20; if $q_{02} = 4/11$, then the minimum pole pairs is 55, which is obviously not suitable for motors with certain size requirements. Therefore, some pole-slot combination can be applied to the traditional fractional slot motor but not to the proposed motor, which has a dual-stator.

If the inner and outer motors of the DS-PMDDM adopt the same pole-slot combination, greater flexibility in the selection of pole pairs is obtained. When the pitch of the coil $y_1 = (1 - 1/v)\tau$ (where v is the harmonic order and τ is the pole distance of the motor), v can be effectively eliminated. Table 1 lists the short distance coefficient, distribution

TABLE 1. The coefficients corresponding to different q values and the harmonic reduction when the winding pitch is 1.

q	y_1/τ	K_{y1}	K_{q1}	K_{dp1}	Harmonic reduction
1/2	2/3	0.866	1	0.866	3
2/5	5/6	0.966	0.966	0.933	5,7
3/8	8/9	0.985	0.960	0.946	9
4/11	11/12	0.991	0.958	0.949	11,13
5/14	14/15	0.995	0.957	0.952	15

coefficient, stator winding factor, and harmonic order that are weakened when y_1 equals 1 but the number of slots per pole per phase is different.

Table 1 shows that, with the decrease in q, the utilization ratio of the winding increases, but at the same time, the order of the harmonics weakened gradually increases. When designing the motor, we try to weaken the influence of low harmonics on its performance. Regardless of whether the symmetrical three-phase winding of the motor adopts the method of triangle connection or star connection, there will be no integer multiple harmonics of third order in its phase electromotive force. Therefore, considering the utilization ratio of the winding and the ability to weaken the harmonic, the number of slots per pole per phase q is chosen as 0.4.

In Table 1, K_{y1} is the short distance coefficient, K_{q1} is the distribution coefficient, and K_{dp1} is the stator winding factor.

IV. ELECTROMAGNETIC FIELD SIMULATION ANALYSIS OF DS-PMDDM

A. MAIN PARAMETERS OF THE DS-PMDDM
Based on the above analysis, a DS-PMDDM for a mine winch with a rated power of 110 kW and a traction force of 60 kN is designed. The main parameters are listed in Table 2.

B. ELECTROMAGNETIC PERFORMANCE
In this section, the electromagnetic field simulation analysis of the designed DS-PMDDM is performed. Fig. 5 and Fig. 6 show that the magnetic field distribution of the designed DS-PMDDM is reasonable, the main magnetic circuit is not seriously saturated, and the magnetic flux leakage is small. The inner and outer motor magnetic circuits form a circuit independently, the waveform of the no-load back EMF is sinusoidal, and the EMF value can reach the design value. Fig. 7 shows the no-load air gap flux density waveform according to the equivalent magnetic circuit method and the finite element method. Fig. 8 shows the output torque of the inner and outer motors, and the torque ripple of the total output torque is 3.19%.

Fig. 7 shows that there is a slight difference between the simplified equivalent magnetic circuit method and the finite element method, especially at the cogging position. This is because, in the calculation of the simplified equivalent magnetic circuit method, the influence of the stator slot on the air-gap flux density cannot be accurately considered, and

TABLE 2. Main parameter of the DS-PMDDM.

Parameter	Value
Rated power of outer motor/kW	110
Rated power of inner motor/kW	65
Rated voltage/V	1140
Slot fill factor of outer motor	0.763
Slot fill factor of inner motor	0.759
Rated speed/(r/min)	48
Core length/mm	600
Outside air-gap/mm	2.0
Inside air-gap/mm	1.5
Number of poles/slots	40/48
Outer motor number of conductors per slot	48
Inner motor number of conductors per slot	54
Outside diameter of outer stator/mm	1000
Inside diameter of outer stator/mm	805
Outside diameter of inner stator/mm	684
Inside diameter of inner stator/mm	470
Thickness of outer PM/mm	12
Pole embrace of outer PM	0.854
Thickness of inner PM/mm	10
Pole embrace of inner PM	0.814
Total weight of PM/kg	176.4
Total weight of steel/kg	1467.3
Total weight of copper/kg	490.2
No-load back EMF of inner motor/V	623.5
No-load back EMF of outer motor/V	634.8
Current density of outer motor/A/mm^2	3.12
Current density of inner motor/A/mm^2	3.69
Armature Thermal Load of outer motor/A^2/mm^3	171.2
Armature Thermal Load of inner motor/A^2/mm^3	158.7
Rated efficiency of outer motor/%	92.5

(a)

(b)

FIGURE 5. The magnetic field of the DS-PMDDM with no-load. (a) distribution of the flux line (b) the map of the flux density distribution.

(a)

(b)

FIGURE 6. No-load back EMF of the DS-PMDDM. (a) inner motor (b) outer motor.

part of the magnetoresistance is ignored. However, the overall trends of the two methods are similar, and the mathematical model derived using the equivalent magnetic circuit method is established.

C. TORQUE-ANGLE CHARACTERISTIC

The torque-angle characteristic plays an important role in PMSMs. The torque-angle characteristic reflects the change in the motor output torque caused by the change in the current vector angle (the angle between the stator current vector and the d-axis positive direction) when the stator current of the motor is fixed. Considering the maximum output current of the controller, the maximum output torque of the motor can be calculated using the torque-angle characteristic to evaluate the operation performance of the motor better. To illustrate the torque-angle characteristics of the DS-PMDDM, the maximum operating current of the motor is determined to be twice the rated current. The torque-angle characteristics of the motor at the rated current and twice the rated current are calculated via the FEM, as shown in Fig. 9.
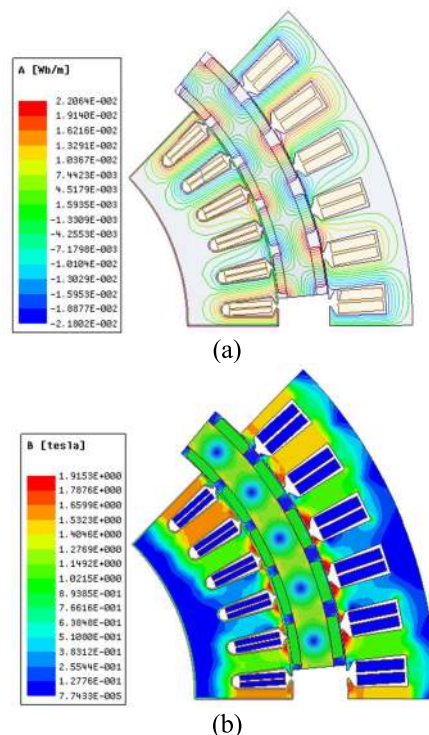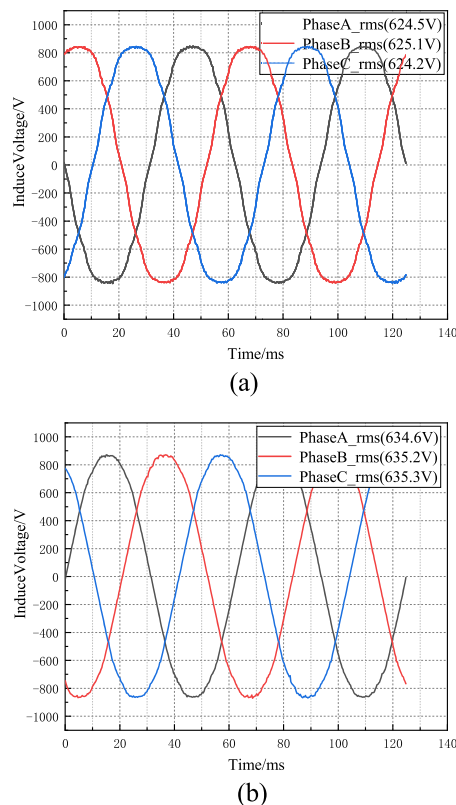
The results show that the output torque increases first and then decreases with increasing phase current angle, and the maximum torque is output when the phase current angle
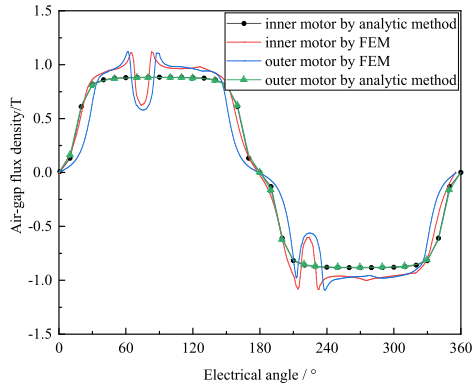
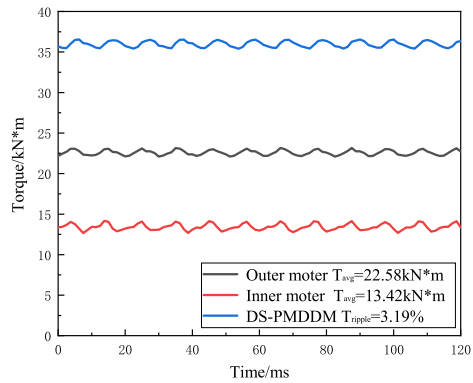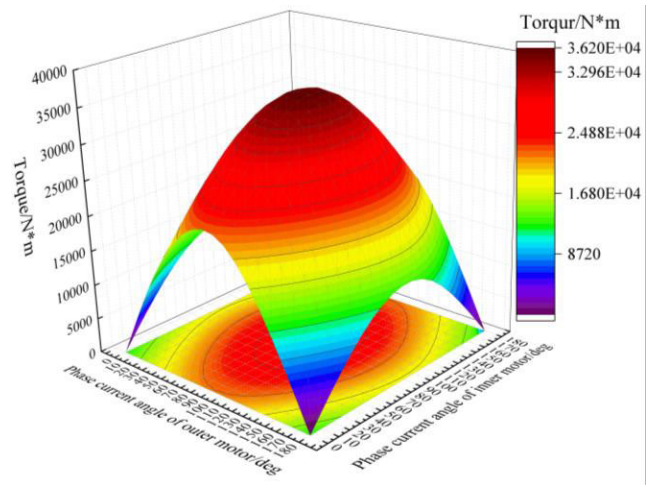**FIGURE 7. No-load air-gap flux density waveform of the DS-PMDDM.**

FIGURE 8. Output torque of the DS-PMDDM.

(a)

(b)

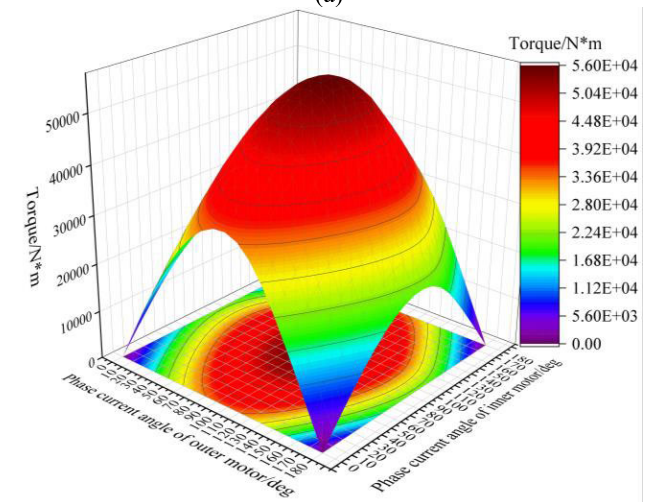**FIGURE 9. Torque-angle characteristics. (a)I=IN (b)I=2∗IN.**

is 90°, which is when the stator current is entirely the q-axis current, because the d-axis reactance equals the q-axis reactance in a surface-mounted PMSM, and the machine has no reluctance torque and a small magnetic flux leakage [22]. When the current increases to twice the rated current, the maximum output torque of the DS-PMDDM is 56.0 kN∗m, which is 1.55-fold that of the rated current. This is because the saturation level of the DS-PMDDM magnetic circuit increases with the current, so the increase in the output torque presents a type of nonlinearity.

D. TEMPERATURE RISE CHARACTERISTIC

The temperature rise characteristic of a motor is one of the important parameters of motor operation. The temperature rise characteristic determines the maximum output power of a motor. Exceeding the specified limit affects the life and reliability of the motor. The insulation grade of the designed DS-PMDDM is H-class, and the cooling mode is water cooling of the outer stator shell. The permanent magnet is segmented along the axial direction. Ignoring the layer insulation and is equivalent to the slot liner and winding after painting as a whole. Fig. 10 shows the overall structure. The loss under the rated condition of the DS-PMDDM calculated via finite element analysis is shown in Table 3. As the inner motor is of a short-time working system, its heat generation rate will be treated equivalently.
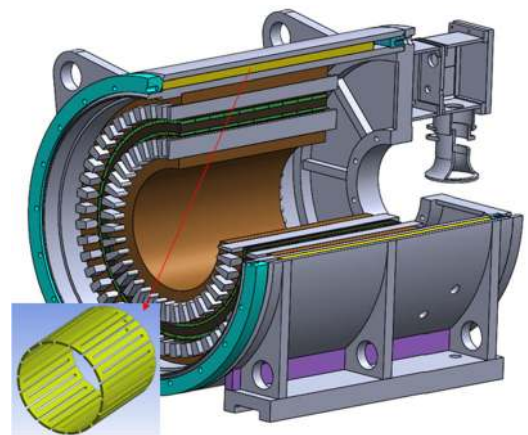

**FIGURE 10. Water-cooling system of the proposed DS-PMDDM.**

The results in Fig. 11 (a) show that the maximum temperature rise of the motor occurs at the end of the stator winding of the outer motor. For the low-speed and high-torque motor, the copper loss of the stator accounts for the main part, but

TABLE 3. Loss calculation value under THE rated condition.

Parameter	Loss
Iron loss of outer motor/W	554.1
Copper loss of outer motor/W	7304.9
Eddy current loss of outer PM/W	1233.9
Iron loss of inner motor/W	590.2
Copper loss of inner motor/W	5592.8
Eddy current loss of inner PM/W	563.3
Mechanical loss/W	875.0
Stray loss of outer motor/W	487.1
Stray loss of inner motor/W	678.0
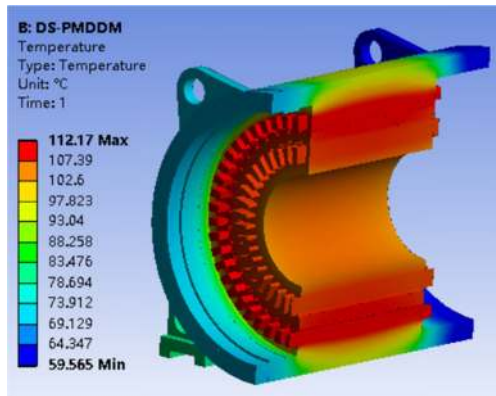
(a)
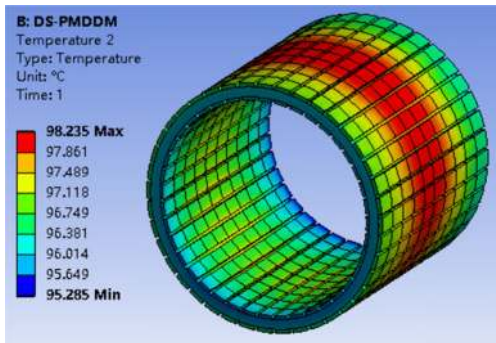
(b)

FIGURE 11. Temperature increase characteristics (a) temperature pattern of the complete machine (b) temperature increase of the PM.

most of the heat is removed by the water cooling of the outer stator shell, and the temperature rise meets the requirements. The inner motor belongs to the short-time working system. When it stops, it belongs to the cooling process, so the temperature rise is limited. The results in Fig. 11 (b) show that the temperature rise of the PM is much lower than the maximum operating temperature of the PM (N38UH). The above results show that the designed water-cooling system of DS-PMDDM meets the requirements of temperature rise performance.

E. TORQUE PERFORMANCE OPTIMIZATION

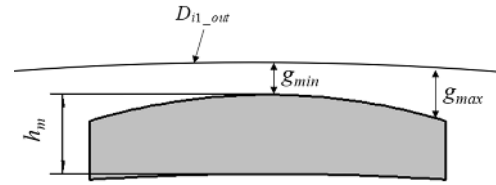Because of the complex structure of the double-stator motor, the performance of the inner and outer motors has a

superimposed effect on the machine. The DS-PMDDM proposed in this paper is used to drive the mine winch, and the high starting torque and low-speed smooth operation are our expectations. Therefore, the torque performance of the motor must be optimized. DS-PMDDM adopts a surface-mounted magnetic pole structure. The shape of the PM is easily and conveniently optimized to make the gap magnetic field close to the sinusoidal shape. The permanent magnet manufacturer directly processes the required shape according to the customer's requirements to reduce the cogging torque and torque ripple. Therefore, as shown in Fig. 12, the nonuniform air gap coefficient K ($K = g_{max}/g_{min}$) of the outer motor is parameterized, and the calculation results are shown in Table 4 (rated current $I_N = 62$ A), and the variations in torque ripple and cogging torque with K are shown in Fig. 13.

FIGURE 12. Optimized permanent magnet shape of the outer motor.

TABLE 4. Torque performance parameter.

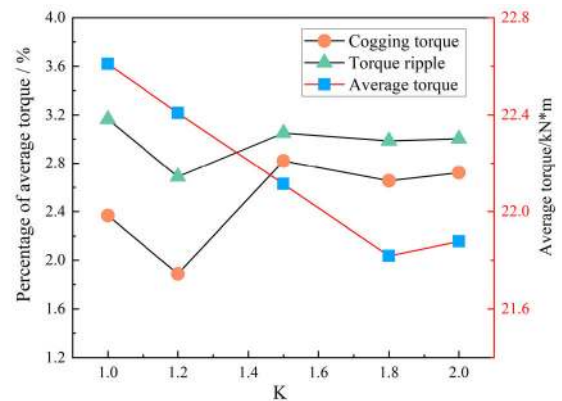| Parameter / K	1	1.2	1.5	1.8	2
Average torque/kN*m	22.6	22.41	22.11	21.82	21.88
Cogging torque/N*m	535	423	595.4	579.5	595.5
Torque ripple/N*m	716	602.6	674.7	651.7	657

FIGURE 13. Variation in the torque ripple and cogging torque with K.

We find that the cogging torque and load torque ripple decrease first and then increase with increasing K, and both of them is at a minimum when $K = 1.2$, while the average torque decreases gradually with the increase of K value.

This is because with the change of K, the sinusoidal and amplitude of the magnetic field established by PM in the air gap also changes. The variation trend of cogging torque in Fig. 13 shows that the waveform of no-load air-gap flux density is closest to sine when $K = 1.2$, and the variation trend of load torque ripple shows that the distortion caused by armature reaction on air gap flux density waveform is the least when $K = 1.2$, which can also be regarded as the waveform distortion rate of load back EMF minimum. Therefore, $K = 1.2$ is taken as the optimal design.

As a torque motor, the inner motor works for a short time when it starts under a heavy load or overload, and its main function is to enhance the torque. Therefore, the inner motor still adopts the original design of $K = 1$ to make the output torque sufficiently large.
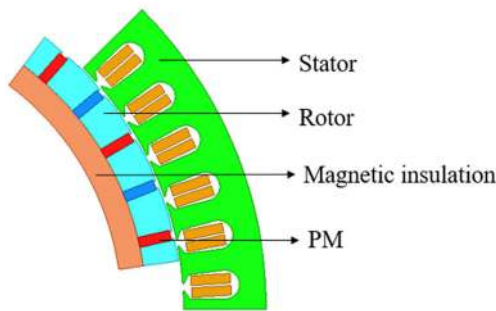

FIGURE 16. Torque-angle characteristics.

FIGURE 14. Finite element calculation model of tangential pole structure PMSM.

FIGURE 17. Torque-angle characteristics.

FIGURE 15. Output torque of the single stator tangential permanent magnet motor.
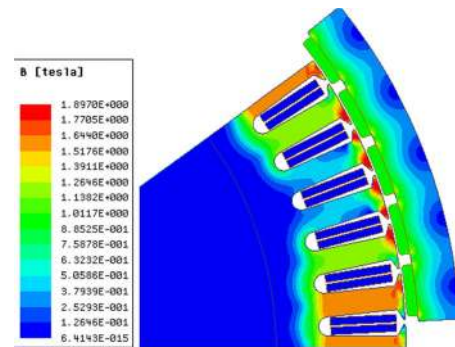
FIGURE 18. Finite element calculation model of the surface-mount outer rotor of PMSM.

V. COMPARISON OF TORQUE PERFORMANCE OF THE DS-PMDDM AND OTHER TYPES OF PMSMs

In this section, the proposed DS-PMDDM is compared with three types of single stator low-speed high-torque permanent magnet motors with different rotor structures. The constraint conditions are identical to the external dimensions of the proposed motor. The simulation results of the different motor rotor types are shown in Fig. 14-19. The motor performance
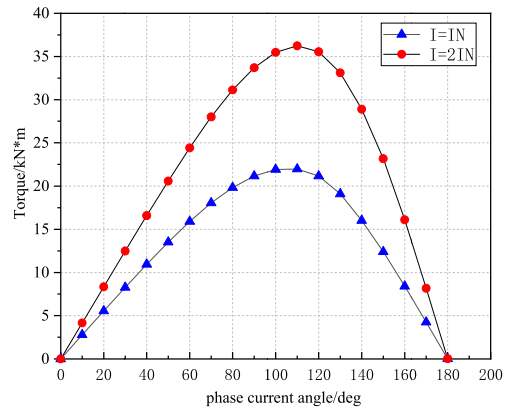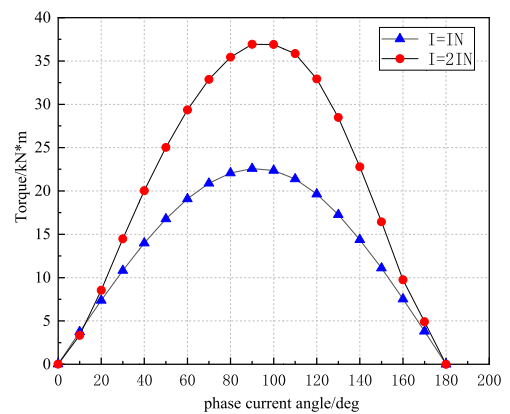
parameters are shown in Table 5. Some parameters of the DS-PMDDM are shown in Table 2.

Table 5 shows that the maximum torque of the DS-PMDDM is 56 kN*m under the same boundary dimension constraint as those of the other motors, which has great advantages compared with other motors because of the torque enhancement of the internal motor.

The rated efficiencies of the four types of motors are almost identical under the same boundary dimension constraint. However, when the user selects the motor, the power
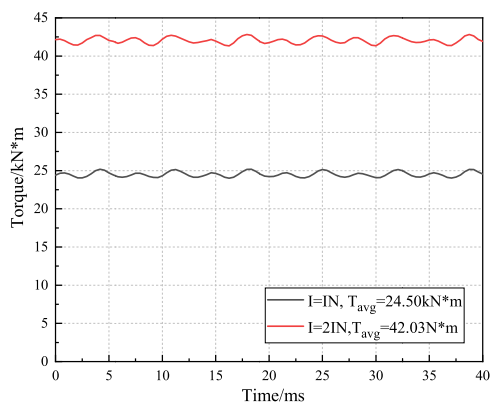
FIGURE 19. Output torque of the single stator surface-mount outer rotor permanent magnet motor with a current angle of 90°.

TABLE 5. Main parameters of Different rotor structures OF PMSMs.

Parameter	DS-PMDDM	Tange ntial	Surface-mount inner rotor	Surface-mount outer rotor
Output power/kW	175	110	110	125
Outside diameter of stator/mm	1000	1000	1000	905
Core Length/mm	600	600	600	600
Number of poles/slots	40/48	40/48	40/48	60/72
Slot fill factor	-	0.763	0.764	0.773
Current density/A/mm^2	-	3.1	3.1	3.01
Thickness of PM/mm	-	12	12	10
Width of PM/mm	-	38	50	37.6
Max torque(2*IN)/kN*m	56	36.35	36.9	42.0
Rated efficiency/%	92.5	92.5	92.3	92.8
Thermal load/A^2/mm^3	-	170.2	172.1	157.6

of the motor is determined according to the extreme working conditions of the load, and a certain margin is reserved; that is, the motor has a certain power redundancy, especially for the winch drive motor, which is often started with a heavy load. On the other hand, to ensure the reliability of the motor and increase its starting capacity and overload force, a certain margin is usually reserved based on the required power. Therefore, more than 90% of the actual operation of the motor power is less than 70% of the rated power, or even lower, and the motor is not fully used. However, for the proposed DS-PMDDM, the outer motor meets the rated load demand, and leaving a margin in the design is unnecessary because the inner motor works under heavy load starting and overload as a torque motor, which makes the proposed motor work

in a higher efficiency range. The motor is fully used, and the internal torque motor does not occupy additional space, which also have great advantages in applications to mine motors.

A. COMPARISON WITH THE SINGLE STATOR TANGENTIAL PERMANENT MAGENT MOTOR

The analysis results in Figs. 15-16 show that the maximum output torque of the motor is at 1.65-fold the rated current, which is larger than the torque multiple of the DS-PMDDM. According to the comparison between Fig. 9 and Fig. 16, although the maximum output torque multiple of the DS-PMDDM is slightly lower than that of the single stator tangential permanent magnet motor, compared with the maximum output torque value, the DS-PMDDM has a great, natural advantage brought by the double-stator structure. Under the condition that the outer dimension of the motor is unchanged, the inner space of the rotor of the low-speed and high-torque motor is reasonably used, which greatly improves the torque density and starting performance of the motor.

B. COMPARISON WITH THE SINGLE STATOR SURFACE-MOUNT INNER ROTOR PERMANENT MAGENT MOTOR

According to the analysis in section IV, under the same boundary dimension constraint of the DS-PMDDM, the torque-angle characteristic of the single stator surface-mount inner rotor permanent magnet motor is equivalent to that of the DS-PMDDM when the current angle of the inner motor is assigned a value of 0°, and the torque characteristic can be obtained, as shown in Figure 17.

When the current is 2∗*IN*, the maximum output torque of the motor is 65.9% of the DS-PMDDM. Although the two motors have identical overall dimensions, the internal space of the single stator motor rotor is only used as the rotor support, which is not fully used.

C. COMPARISON WITH THE SINGLE STATOR SURFACE-MOUNT OUTER ROTOR PERMANENT MAGENT MOTOR

The single stator surface-mount outer rotor motor is compared with the DS-PMDDM, assuming the boundary dimension constraints are identical to those of the DS-PMDDM, and Table 5 shows the main parameters of the motor. The finite element simulation results are shown in Figs. 18-19. The results show that the output torque of the single stator surface-mount outer rotor permanent magnet motor is larger than those of the single stator tangential permanent magnet motor and the single stator surface-mount inner rotor permanent magnet motor. This is because the armature diameter of the outer rotor motor is larger, so the power density of the motor is larger under identical motor boundary dimension constraints. However, compared with those of the DS-PMDDM, the rated torque and the maximum output torque are lower.

VI. COST COMPARISON

In this section, the proposed DS-PMDDM is compared with three types of single stator low-speed high-torque permanent magnet motors with different rotor structures. Under the condition that the maximum output torques are identical, the amount of electromagnetic materials consumed is calculated, and their costs are further compared. The main design parameters and electromagnetic material consumption of different types of motors are shown in Table 6; the maximum outer diameter limit remains 1000 mm. The parameters of the DS-PMDDM are shown in Table 2, and the weight of the electromagnetic materials are shown in Fig. 20. The cost of the electromagnetic materials for the four types of motors is shown in Fig. 21.

FIGURE 21. Electromagnetic cost comparison.

TABLE 6. Costing data of different types of motors.

Parameter	Tangential	Surface-mount inner rotor	Surface-mount outer rotor
Rated torque/k*Nm	34.86	35.07	35.60
Stator outside diameter/mm	1000	1000	905
Stator inside diameter/mm	805	805	660
Core Length/mm	920	950	890
Turns-in-series per-phase	232	232	224
Slot fill factor	0.780	0.775	0.785
Current density/ A/mm^2	2.95	2.97	2.89
Rated efficiency/%	0.925	0.927	0.929
Thickness of PM/mm	12	12	10
Width of PM/mm	38	50	37.6
Weight of PM/kg	125.0	169.8	150.5
Weight of steel/kg	2005	1335	1364
Weight of copper/kg	477.8	478.6	446.1

The comparison results show that, among the four types of motors, the DS-PMDDM consumes the most electromagnetic materials with the highest cost, while the surface-mounted outer rotor permanent magnet motor has the lowest electromagnetic cost; the tangential structure motor uses the least amount of permanent magnet, while the silicon steel sheet uses the most because the rotor pole material is also silicon steel sheet. In general, the electromagnetic cost of the DS-PMDDM is slightly higher than those of the other types of motors, but the difference is not substantial. In contrast to the surface mounted outer rotor permanent magnet motor with the lowest electromagnetic cost, the DS-PMDDM axial core length is only 600 mm and the volume can be reduced by 32.6% because of the double-stator structure of the proposed motor, which is more meaningful for use as a mine motor.

VII. CONCLUSION

In this paper, a double-stator permanent magnet direct drive motor with inner enhanced torque is proposed. It is characterized by a torque motor for the inner motor and a direct drive motor for the outer motor. Compared with the traditional single stator permanent magnet motor, this motor has a higher torque density, a higher starting torque, and a higher utilization ratio of the electric machine. The design principles of the size equation, electromagnetic parameters, and pole-slot combination are illustrated and analyzed by simulation in detail. Moreover, the distribution characteristics of the temperature increase are summarized via a finite element analysis. The proposed water-cooling system effectively reduces the temperature increase in the DS-PMDDM and ensures the stable operation of the proposed motor. Finally, the torque performance and electromagnetic materials cost of the proposed motor and single stator motor with different rotor types are compared under the condition of boundary dimension constraint and output torque constraint. The results show that the maximum output torque and motor volume of the DS-PMDDM have great advantages under identical maximum current limiting amplitudes, and the costs of the electromagnetic materials are almost identical, which proves that the DS-PMDDM has the advantages of a high torque

FIGURE 20. Electromagnetic material consumption of different types of motors.

density and strong heavy load starting ability. In addition, the proposed motor has a higher efficiency range in actual operation conditions, there is no large power redundancy in the motor selection, and the control is flexible. It provides a solution for many special industrial applications, such as the mine winch drive system, which requires a low-speed and high-torque direct drive operation as well as frequent heavy load starting.

REFERENCES

[1] F. Chai, S. Cui, and S. Cheng, "Performance analysis of double-stator starter generator for the hybrid electric vehicle," *IEEE Trans. Magn.*, vol. 41, no. 1, pp. 484–487, Jan. 2005.

[2] S. Asgari and M. Mirsalim, "A novel dual-stator radial-flux machine with diametrically magnetized cylindrical permanent magnets," *IEEE Trans. Ind. Electron.*, vol. 66, no. 5, pp. 3605–3614, May 2019.

[3] C. Feng, X. Jing, G. Bin, C. Shukang, and Z. Jiange, "Double-stator permanent magnet synchronous in-wheel motor for hybrid electric drive system," *IEEE Trans. Magn.*, vol. 45, no. 1, pp. 278–281, Jan. 2009.

[4] H. Yang, S. Lyu, Z. Q. Zhu, H. Lin, S. Wang, S. Fang, and Y. Huang, "Novel dual-stator machines with biased permanent magnet excitation," *IEEE Trans. Energy Convers.*, vol. 33, no. 4, pp. 2070–2080, Dec. 2018.

[5] S. Yang, F. Zhang, Z. Zhang, and H. Liu, "Design of double stator permanent magnet synchronous motor with low speed large torque," in *Proc. IEEE Student Conf. Electr. Mach. Syst.*, Dec. 2018, pp. 1–6.

[6] C. Liu, K. T. Chau, and Z. Zhang, "Novel design of double-stator single-rotor magnetic-geared machines," *IEEE Trans. Magn.*, vol. 48, no. 11, pp. 4180–4183, Nov. 2012.

[7] C. C. Awah and Z. Q. Zhu, "Comparative study of high performance double-stator switched flux permanent magnet machines," in *Proc. IEEE Vehicle Power Propuls. Conf. (VPPC)*, Oct. 2016, pp. 1–6.

[8] D. Kim, H. Hwang, S. Bae, and C. Lee, "Analysis and design of double stator flux-switching permanent magnet machine using ferrite magnet in hybrid electric vehicles," *IEEE Trans. Magn.*, vol. 52, no. 7, pp. 1–4, Feb. 2016.

[9] W. Zhao, T. A. Lipo, and B.-I. Kwon, "Dual-stator two-phase permanent magnet machines with phase-group concentrated-coil windings for torque enhancement," *IEEE Trans. Magn.*, vol. 51, no. 11, pp. 1–4, Nov. 2015.

[10] F. Zhao, T. A. Lipo, and B.-I. Kwon, "A novel dual-stator axial-flux spoke-type permanent magnet Vernier machine for direct-drive applications," *IEEE Trans. Magn.*, vol. 50, no. 11, pp. 1–4, Nov. 2014.

[11] F. Chai, S. Cui, and S. Cheng, "Torque analysis of double-stator permanent-magnet motor," *J. Harbin Inst. Technol.*, vol. 9, no. 4, pp. 411–414, 2002.

[12] Y. Wang and M. W. Cheng Hua, "Analysis and optimization of split ratio of double stator permanent magnet BLDCM," in *Proc. CSEE*, vol. 30, no. 30, pp. 62–67, Oct. 2010.

[13] Y. Wang, M. Cheng, Y. Feng, and G. Zou, "Design and electromagnetic characteristics analysis of double stator permanent magnet brushless motor for power distribution," *J. Electrotechnics*, vol. 25, no. 10, pp. 37–43, Oct. 2010.

[14] L. Zhu, S. Z. Jiang, Z. Q. Zhu, and C. C. Chan, "Analytical methods for minimizing cogging torque in permanent-magnet machines," *IEEE Trans. Magn.*, vol. 45, no. 4, pp. 2023–2031, Apr. 2009.

[15] D. Zarko, D. Ban, and T. A. Lipo, "Analytical solution for cogging torque in surface permanent-magnet motors using conformal mapping," *IEEE Trans. Magn.*, vol. 44, no. 1, pp. 52–65, Jan. 2008.

[16] J. F. Gieras, "Analytical approach to cogging torque calculation of PM brushless motors," *IEEE Trans. Ind. Appl.*, vol. 40, no. 5, pp. 1310–1316, Sep. 2004.

[17] L. Xiao, J. Li, R. Qu, Y. Lu, R. Zhang, and D. Li, "Cogging torque analysis and minimization of axial flux PM machines with combined rectangle-shaped magnet," *IEEE Trans. Ind. Appl.*, vol. 53, no. 2, pp. 1018–1027, Mar. 2017.

[18] Y. Meng, K. Lu, L. Wu, and H. Yin, "Reduction methods using canceling effect for cogging torque in dual-stator PM synchronous machines," in *Proc. IEEE Int. Electr. Mach. Drives Conf. (IEMDC)*, May 2019, pp. 714–720.

[19] S. Huang, J. Luo, F. Leonardi, and T. A. Lipo, "A general approach to sizing and power density equations for comparison of electrical machines," *IEEE Trans. Ind. Appl.*, vol. 34, no. 1, pp. 92–97, Jan. 1998.

[20] A. M. El-Refaie, T. M. Jahns, and D. W. Novotny, "Analysis of surface permanent magnet machines with fractional-slot concentrated windings," *IEEE Trans. Energy Convers.*, vol. 21, no. 1, pp. 34–43, Mar. 2006.

[21] A. M. EL-Refaie and T. M. Jahns, "Optimal flux weakening in surface PM machines using fractional-slot concentrated windings," *IEEE Trans. Ind. Appl.*, vol. 41, no. 3, pp. 790–800, May 2005.

[22] Y.-P. Yang and M.-T. Peng, "A surface-mounted permanent-magnet motor with sinusoidal pulsewidth-modulation-shaped magnets," *IEEE Trans. Magn.*, vol. 55, no. 1, pp. 1–8, Jan. 2019.

JIAXU ZHANG received the B.S. degree in electrical engineering and automation from the Shenyang University of Technology, Shenyang, China, in 2016, where he is currently pursuing the Ph.D. degree in electrical engineering. His research interest includes design and control of permanent magnet motor.

BINGYI ZHANG received the B.S., M.S., and Ph.D. degrees in electrical engineering from the Shenyang University of Technology, Shenyang, China, in 1982, 1987, and 2007, respectively. He is currently a Professor with the Shenyang University of Technology. His research interests include design and optimization of electrical machines, low-speed high-torque drive systems, and power system automation.

GUIHONG FENG received the B.S. degree in electrical engineering from the Shenyang University of Technology, Shenyang, China, in 1985, and the M.S. degree in electric drive and automation from Northeastern University, Shenyang, in 1994. She is currently a Professor with the Shenyang University of Technology. Her research interests include design and optimization of electrical machines, low-speed high-torque drive systems, and power system automation.

BAOPING GAN received the B.S. degree in electrical engineering and automation from the Shenyang University of Technology, Shenyang, China, in 2016, where he is currently pursuing the Ph.D. degree in electrical engineering. His research interest includes design and control of permanent magnet motor.

• • •